

# Characteristics of the rotor R4-01 for the O4 NCal system VIR-0591A-22

Eddy Dangelser, Dimitri Estevez, Hubert Kocher, Benoit Mours,  
Mehmet Ozturk, Antoine Syx

IPHC-Strasbourg

June 03, 2022

## Contents

<b>1</b>	<b>Introduction</b>	<b>2</b>
<b>2</b>	<b>Measurement method</b>	<b>3</b>
2.1	Thermal effects and density . . . . .	4
<b>3</b>	<b>Raw measurements of the rotor</b>	<b>4</b>
<b>4</b>	<b>Extracting the geometrical parameters</b>	<b>5</b>
4.1	Thickness . . . . .	5
4.2	Radius . . . . .	6
<b>5</b>	<b>Characterization of the rotor using a simple model</b>	<b>7</b>
5.1	Theoretical model of the rotor . . . . .	7
5.2	Thickness . . . . .	7
5.3	Radius . . . . .	7
5.4	Expected NCal signal and uncertainties . . . . .	8
<b>6</b>	<b>Design of a counterweight</b>	<b>9</b>
6.1	The circular plate on the rotor . . . . .	9
6.2	Preliminary counterweight . . . . .	10
6.2.1	Design of a preliminary counterweight . . . . .	10
6.2.2	Model of the center of gravity using moments . . . . .	11
6.3	Data taking from the position sensors . . . . .	12
6.4	Counterweight tuning . . . . .	13
6.4.1	Machined circular plate . . . . .	13
6.4.2	Determination of the geometry of the counterweight . . . . .	13
6.4.3	Testing the theoretical geometry . . . . .	14

<i>VIR-0591A-22</i>	<i>Characteristics of the rotor R4-01 for the O4 NCal system</i>	2
6.4.4	Final corrections on the counterweight . . . . .	14
<b>7</b>	<b>Characterization of the rotor using an advanced model</b>	<b>15</b>
7.1	Thickness . . . . .	15
7.2	Radius . . . . .	15
7.3	Chamfers on the rotor . . . . .	16
7.4	Expected NCal signals and uncertainties . . . . .	16
7.4.1	Advanced model including chamfers and counterweight . . . . .	16
7.4.2	Chamfers effect . . . . .	18
7.4.3	Counterweight effects using FROMAGE . . . . .	18
7.4.4	Opening angles and sectors asymmetry . . . . .	19
7.4.5	Uncertainties . . . . .	20
<b>A</b>	<b>Appendix</b>	<b>22</b>

# 1 Introduction

The challenge of the NCal system for O4 is to improve the NCal signal uncertainty. This can be achieved by reducing uncertainties on the rotor parameters such as the density of the material discussed in [VIR-0160A-22](#), the thickness or the radius of the sectors.

Figure 1 shows an isometric view and pictures of both faces of the O4 rotor design. The drawings are attached at the end of this note.

The rotor has been engraved IPHC-R4-01 on a side and sandblasted on the other side as shown in figure 2.

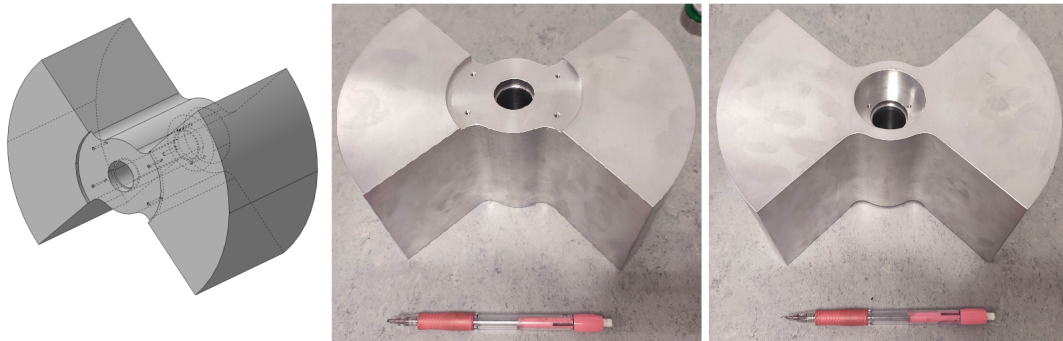


Figure 1: From left to right, isometric view of the rotor, picture of the up face, picture of the down face.

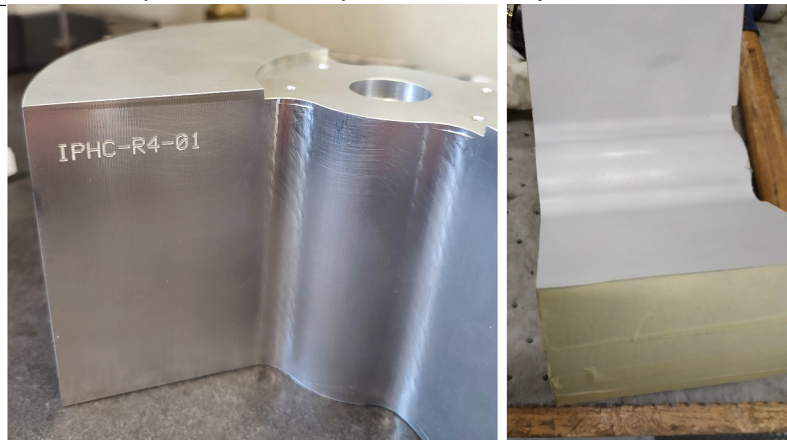


Figure 2: Left shows the engraving made on a side of the rotor, right shows the sandblasting made on the other side.

## 2 Measurement method

To determine the geometry of the rotor, several measurement points were used to compute the thickness of the sectors as shown in figure 3. Since the strain on the mirror induced by the rotor will come from the sectors, we need to measure the thickness of both sectors as well as the outer and inner diameters. The central part is not affecting the signal since it is a full cylinder. The outer diameter was measured in  $4 \times 2 = 8$  points and the inner diameter using 4 points.

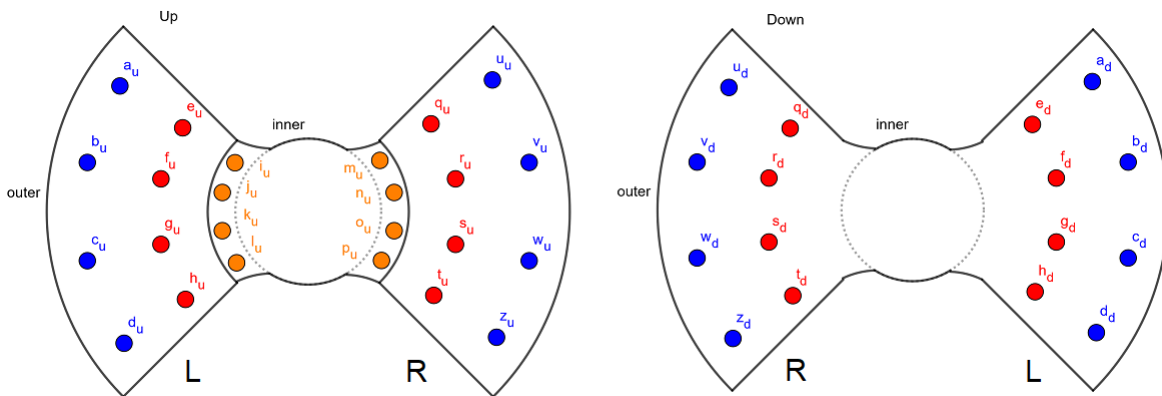


Figure 3: Outline of the faces of the rotor with the measurement points. Left figure is face up, right figure is face down. Sectors have been labelled L for left sector and R for right sector.

The tool used to measure the thickness and the outer diameter is a measuring column "DIGIMAR CX1" (see [VIR-0160A-22](#)) with a given precision of  $2 + L/600 \mu\text{m}$  ( $L$  the measured length in mm). A vernier caliper "TESA-CAL IP67" with a precision of  $20 \mu\text{m}$  was used to measure the inner diameter.

The measuring column is operated on a metrology table, different measurements were made to check the flatness on a surface roughly equivalent to the rotor layout. The value range from 0 to  $7 \mu\text{m}$ . The rms of the 11 values is  $2.0 \mu\text{m}$ .

## 2.1 Thermal effects and density

As discussed in [VIR-0160A-22](#), the thermal effects on the aluminum 7075 must be taken into account (23.6  $\mu\text{m}/\text{m}/^\circ\text{C}$ ).

A reference temperature of 21.5°C was chosen to express the density of the material. The temperature inside the NE building might fluctuate around 21.5°C. The temperature of the motor can increase by up to several tens of degrees depending on the rotation speed. This will increase the rotor temperature. The strains computation has been made assuming a reference temperature of 23°C. They will have to be corrected using eq. (2) for the true operating temperature. We expect to know this temperature with an uncertainty of  $\pm 3^\circ\text{C}$ .

The uncertainty on the strain  $h$  is the following:

$$\begin{aligned} h &\propto \rho_{rot} b r_{max}^4 \\ &\propto \frac{m r_{max}^2}{\pi} \end{aligned} \quad (1)$$

Using  $r(T) = r(1 + \alpha_T)$  (with the temperature factor  $\alpha_T = C_T(T - T_{ref})$ ) we have:

$$\begin{aligned} h(T) &\propto r_{max}^2(T) \\ &\propto r_{max}^2(1 + \alpha_T)^2 \end{aligned} \quad (2)$$

We compute the relative uncertainty of  $h$  on the temperature  $T$ :

$$\left| \frac{\partial h}{\partial T} \right| \frac{\Delta T}{h} = \frac{2C_T}{1 + C_T(T - T_{ref})} \Delta T \quad (3)$$

The density of the rotor R4-01 is then  $2808.0 \pm 0.2 \text{ kg}\cdot\text{m}^{-3}$ . This density is measured in air, if the rotor is used under vacuum, the density should be increased by the air density ( $\rho_{air} = 1.3 \text{ kg}\cdot\text{m}^{-3}$ ).

## 3 Raw measurements of the rotor

This section presents the raw measurements made on the rotor at the ambient temperature of 20.1°C. Table 1 shows the thickness measurements according to the measurement points shown in figure 3. The rotor is laying on the table. The rotor surface as well as the table are not perfectly flat. Some space could be present in between that should be subtracted when computing the rotor thickness as discussed later.

Measurement point	L sector		Measurement point	R sector	
	Up	Down		Up	Down
a	104.353	104.339	q	104.319	104.314
b	104.338	104.330	r	104.309	104.308
c	104.325	104.316	s	104.303	104.302
d	104.312	104.302	t	104.299	104.300
e	104.325	104.325	u	104.326	104.326
f	104.314	104.314	v	104.316	104.315
g	104.308	104.308	w	104.303	104.303
h	104.304	104.306	z	104.292	104.294
i	101.269		m	101.262	
j	101.262		n	101.256	
k	101.257		o	101.251	
l	101.252		p	101.248	

Table 1: Raw measurements of the height in mm for each point at 20.1°C on L and R sectors of R4-01.

Table 2 displays the diameter measurements. The measurements were made on 4\*2 diameters (two parts of each diameter, the up and down sides of the rotor).

Measurement point	Up	Down
1	208.046	208.055
2	208.047	208.060
3	208.054	208.053
4	208.044	208.057

Table 2: Raw measurements of the diameter in mm for each point at 20.1°C on R4-01.

Measurements were made on the inner radius  $r_{min} = 28.93$  mm and the up face recess radius  $r_{recess} = 39.99$  mm. These values were measured using the vernier caliper and are the same for a temperature of 21.5°C.

## 4 Extracting the geometrical parameters

### 4.1 Thickness

We need to correct the possible gap between the rotor and the measuring table. Assuming that the table is flatter than the rotor surface we can extract the gap from the measurement of the top surface considering the plane tangents to the highest points (asking them to be on both sectors). For this rotor these points are a, b and u from figure 3. Using the measurements in table 1 we can compute a plane equation for each side of the rotor in cartesian coordinates:

$$\text{Up plane equation : } z = -1.85 \times 10^{-4}x + 5.49 \times 10^{-4}y + 104.32 \quad (4)$$

$$\text{Down plane equation : } z = -8.83 \times 10^{-5}x + 3.21 \times 10^{-4}y + 104.33 \quad (5)$$

Using eqs. (4) and (5) the gap can be determined, see table 3. The rms of the gap is 8.2  $\mu\text{m}$ .

Measurement point	L sector		Measurement point	R sector	
	Up	Down		Up	Down
a	0	0	q	9	2
b	0	0	r	7	-1
c	3	-6	s	6	-7
d	6	-13	t	3	-12
e	6	13	u	0	0
f	11	15	v	0	-10
g	10	9	w	1	-16
h	5	0	z	1	-20

Table 3: Gap computed in  $\mu\text{m}$  on up and down sides of both sectors of R4-01.

We can then compute the rotor thickness for each point by removing these gaps. If one of the raw values is lower than the corrected thickness we take this lowest value. The value of each point is shown in table 4 at 21.5°C.

Measurement point	L sector	Measurement point	R sector
a	104.346	q	104.321
b	104.337	r	104.315
c	104.317	s	104.303
d	104.296	t	104.295
e	104.332	u	104.333
f	104.321	v	104.312
g	104.315	w	104.294
h	104.311	z	104.281
i	101.276	m	101.269
j	101.269	n	101.263
k	101.264	o	101.258
l	101.259	p	101.255

Table 4: Measurements of the thickness in mm for each point at 23°C on L and R sectors of R4-01.

## 4.2 Radius

Using comparators while the rotor is rotating on its axis we can determine the deformation on both sectors and compute different radii values. Table 5 shows the raw measurements using comparators on L and R sectors. The measurements were made on the up and down sides of L and R sectors using two comparators for a total of  $5 \times 2 \times 2 = 20$  points (the first and last points are near the edge of the sectors).

Measurement point	L sector		R sector	
	Up	Down	Up	Down
A	0	-5	20	0
B	20	10	25	0
C	30	20	35	0
D	20	10	0	0
E	0	-5	0	0

Table 5: Raw measurements in  $\mu\text{m}$  of the comparators for the L and R sectors of R4-01.

The zeroing of the comparators was made arbitrarily close to the edge of the sector. The offsets shown in table 5 are measured relative to this reference.

To compute the radius per measurement point we use the following process: First we compute the mean deformation for one comparator. Then we remove this mean deformation to each measurement of this comparator. The corrected shift value is added to the mean radius of 104.029 mm computed using table 2 at 21.5°C. This process is repeated for each comparator. The final radius for each point are shown in table 6.

Measurement point	L sector		R sector	
	Up	Down	Up	Down
A	104.007	104.006	104.027	104.021
B	104.027	104.021	104.032	104.031
C	104.037	104.031	104.042	104.036
D	104.027	104.021	104.032	104.031
E	104.007	104.006	104.027	104.021

Table 6: Radius measurements in mm at 20.1°C for the L and R sectors of R4-01.

We found the sectors to be in an elliptical shape as shown in an amplified representation in figure 4. The general shape of up and down sectors is represented as one unique radius for this representation.

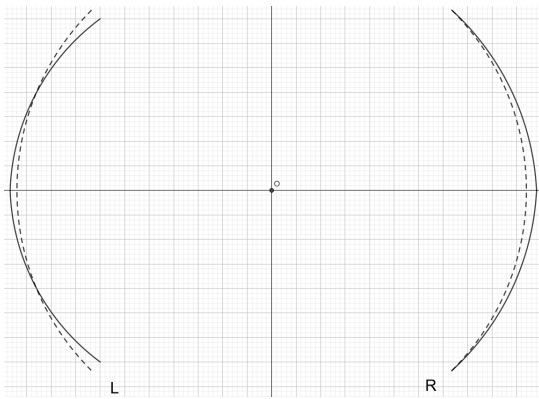


Figure 4: Outline of the shape of the L and R sectors radii. The dashed lines represent the mean diameter of the rotor, the plain lines represent the amplified deformation determined using comparators.

## 5 Characterization of the rotor using a simple model

### 5.1 Theoretical model of the rotor

Using the drawing values of the rotor we have a thickness of 104.4 mm and a radius of 104 mm for both sectors.

Using FROMAGE v1r2 (see [VIR-0759B-20](#)) we compute a theoretical value for the rotor with these values. A config file used to compute an advanced rotor model is shown at the end of this note. We obtain the following  $2f$  strain signal:

$$\text{strain}(2f) = \frac{2.1200 \times 10^{-18}}{(2f_{rot})^2}$$

This strain value will be compared to models based on the measurements of the rotor.

### 5.2 Thickness

A simple model can be used to determine a mean value for the thickness and its uncertainty.

As shown on figure 3, a total of 16 points were used to compute the thickness of each sector. In this case we will not consider the inner points so that we obtain uniform sectors.

For the simple model we take the thickness as the mean value of table 4: 104.314 mm at 23°C. Since we have a limited number of measurement points, to be conservative we take the thickness uncertainty as the rms of table 4 (17.6  $\mu\text{m}$ ) to which we add linearly the metrology table uncertainty (2  $\mu\text{m}$ ) and the tool uncertainty (2.2  $\mu\text{m}$ ). Therefore, for this simple model, the thickness is  $104.314 \pm 0.022$  mm.

### 5.3 Radius

For the simple model we take the radius as the mean value of table 6: 104.033 mm at 23°C. Using a linear sum of the rms of table 6 (10.6  $\mu\text{m}$ ) and the tool uncertainty (2.4  $\mu\text{m}$ ) we take an uncertainty of 12.9  $\mu\text{m}$  on the mean radius.

We have to point out that we do not take into account the fact that the sectors might not be centered on the same axis. Therefore the uncertainty might be underestimated. We will then consider each sector individually later.

## 5.4 Expected NCal signal and uncertainties

The geometry used to describe the rotor as a simple model is represented in figure 5.

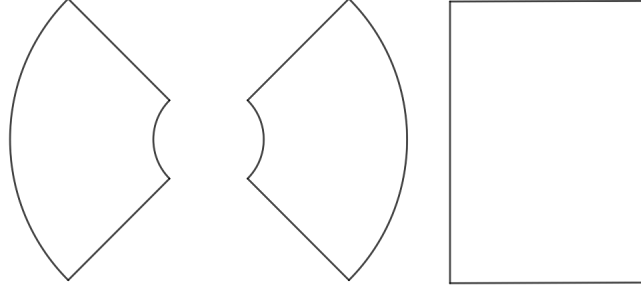


Figure 5: Simple model geometry used to describe the rotor. Left is a front view, right is a side view.

Using the analytical equation of the strain at  $2f$  (see [Newtonian calibrator tests during the Virgo O3 data taking](#)):

$$\text{strain}(2f) = \frac{9G\rho_{rot} b \sin(\alpha)(r_{max}^4 - r_{min}^4)}{32\pi^2(2f)^2 d^4 L} \cos(\phi) \left[ 1 + \frac{25}{54d^2} \frac{(r_{max}^6 - r_{min}^6)}{(r_{max}^4 - r_{min}^4)} + \left( \frac{45}{8} \sin(\phi)^2 - \frac{5}{2} \right) \left( \frac{r_{mir}}{d} \right)^2 + \left( \frac{15}{8} \cos(\phi)^2 - \frac{25}{24} \right) \left( \frac{x_{mir}}{d} \right)^2 - \frac{25}{72} \left( \frac{b}{d} \right)^2 \right] \quad (6)$$

with:

- $G$  the gravitationnal constant
- $\rho_{rot}$  the density of the rotor
- $b$  the thickness of the rotor
- $\alpha$  the opening angle of the rotor
- $r_{max}$  and  $r_{min}$  the outer and inner radius of the rotor
- $f$  the rotor frequency
- $\phi$  the rotor angle from the beam axis
- $L$  the interferometer arm length
- $r_{mir}$  the radius of the mirror
- $x_{mir}$  the thickness of the mirror

We compute with our parameters ( $d = 1.7$  m and an angle  $\phi = 34.7^\circ$ ):  $\text{strain}(2f) = \frac{2.1207 \times 10^{-18}}{(2f_{rot})^2}$ .

Using FROMAGE on this geometry we compute the following strains on the mirror at a distance of 1.7m and an angle of  $34.7^\circ$ :

- $\text{strain}(1f) = \frac{1.28 \times 10^{-30}}{(1f_{rot})^2}$
- $\text{strain}(2f) = \frac{2.1209 \times 10^{-18}}{(2f_{rot})^2}$



$$\bullet \text{ strain}(3f) = \frac{1.76 \times 10^{-30}}{(3f_{rot})^2}$$

We notice that the 2f strain signal has the largest amplitude at  $10^{-18}$ . Both sectors being the same height and radius the only expected significant signal is the 2f. The 1f and 3f strain signals are at the level of the numerical noise of the simulation. This result is in agreement with a simple rotor model.

Comparing the analytical strain (eq. (6)) at 2f with FROMAGE we obtain a relative deviation of 0.009%.

The uncertainties considered on the 2f signal for this model are displayed in table 7.

R4-01 rotor parameter simple model (23°C)			NCal 2f signal uncertainty	
name	value	uncertainty	formula	value (%)
Density $\rho$ (kg.m <sup>-3</sup> )	2808.3	0.2	$\delta\rho/\rho$	0.007
Thickness $b$ (mm)	104.311	$2.2 \times 10^{-2}$	$\delta b/b$	0.021
$r_{max}$ (mm)	104.029	$1.3 \times 10^{-2}$	$4\delta r_{max}/r_{max}$	0.050
$G$ (m <sup>3</sup> .kg <sup>-1</sup> .s <sup>-2</sup> )	$6.67430 \times 10^{-11}$	$1.5 \times 10^{-15}$	$\delta G/G$	0.002
Temperature $T$ (°C)	23	3	$\frac{\partial h}{\partial T} \frac{\Delta T}{h}$	0.014
Total uncertainty from the rotor (quadratic sum)				0.056

Table 7: Uncertainties on the amplitude of the calibration signal at 2f from the R4-01 rotor simple model geometry.

## 6 Design of a counterweight

One of the challenge of the NCal is to be able to produce a reliable system. This mainly concerns the rotors and ball bearings for a 24/7 use. To increase the reliability of the system we balance the rotor to minimize the vibrations.

To measure the slight asymmetry of the rotor we take advantage of the low resonance frequency of the NCal suspension. We measure the recoil displacement using the position sensors on the reference plate. These measurements are made at a fixed frequency of 14 Hz which is away from suspension resonances. Before any balancing we measured an amplitude of 13  $\mu\text{m}$ . This value revealed that the center of gravity of the rotor was not centered on the axis. This section shows the method used to correct this unbalance and the results after a correction using a counterweight mounted on the rotor.

### 6.1 The circular plate on the rotor

A circular metal plate was originally designed to be mounted on the central part of the rotor (figure 6) with a hole so that a photodiode allows us to compute the frequency of the rotor. This plate is fixed on the rotor using four metal screws. The geometry of the screw holes on the rotor is shown on figure 7, considering the cartesian coordinate system the angle from each screw to the horizontal axis  $x$  is  $\theta = 30^\circ$ .

To counterbalance the rotor during its rotation, an open angle counterweight can replace the circular plate to correct the center of gravity back to the axis.

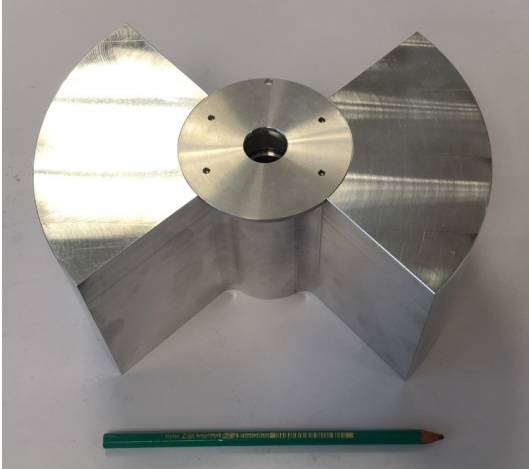
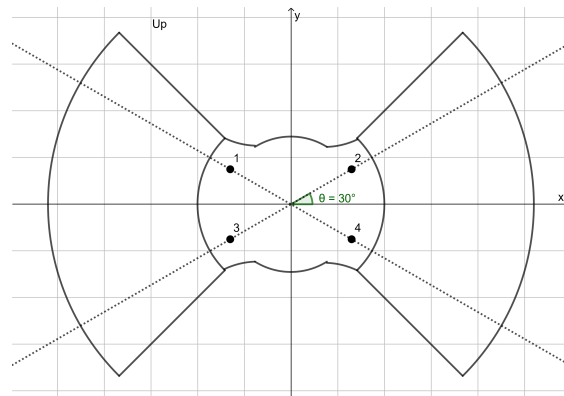


Figure 6: Circular metal plate layed on the up face of the rotor with four screw holes and the photodiode hole visible.

Figure 7: Representation of the up face of the rotor with the screw holes labelled from 1 to 4 and the polar angle  $\theta$ .



In this part we will discuss of a semi circular aluminum plate machined as a preliminary counterweight to determine the correction to apply on the rotor.

## 6.2 Preliminary counterweight

### 6.2.1 Design of a preliminary counterweight

A semi circular plate has been machined with screw holes every  $15^\circ$  as shown in figure 8, this small angle incrementation would allow us to make different tests with the counterweight placed at different angles on the rotor.

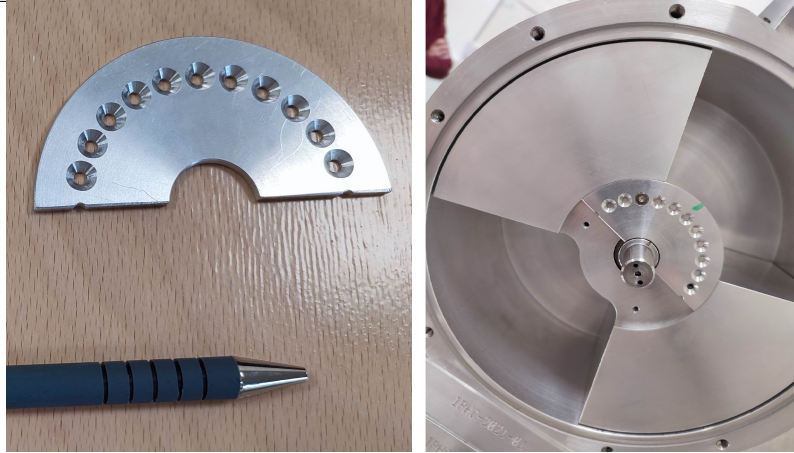


Figure 8: Left is the aluminum counterweight used with screw holes incremented every  $15^\circ$ . Right is the same counterweight mounted on the rotor.

### 6.2.2 Model of the center of gravity using moments

To correct the center of gravity of the rotor we use an analytical model considering the moment  $\mathcal{M}_1$  of the counterweight and the moment  $\mathcal{M}_2$  of the rotor.

Using the equation of the moment  $\mathcal{M}$  where  $m$  is the mass of the object and  $d$  is the distance of the object from the axis:

$$\mathcal{M} = md \quad (7)$$

and the figure 9, we can compute the center of gravity of the two objects system (rotor and counterweight).

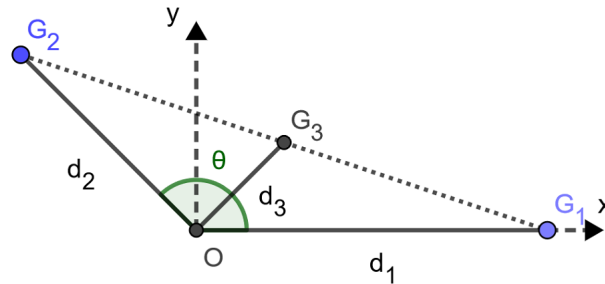


Figure 9: Representation of the center of gravity  $G_3$  of a system composed of two objects 1 and 2 with their respective center of gravity  $G_1$  and  $G_2$  from the point O.

The distance  $d_1$  is the center of gravity of the counterweight that can be set to 1 for the model. The distance  $d_2$  is the center of gravity of the rotor equal to the ratio of the moments  $\mathcal{M}_2$  and  $\mathcal{M}_1$ . The distance  $d_3$  is the center of gravity of the system and can be computed using the polar angle  $\theta$  and the distance  $d_2$ .

We have the following cartesian coordinates  $G_i(x, y)$  for the center of gravity of each object:

$$G_1(d_1, 0) = G_1(1, 0)$$

$$G_2(d_2 \cos \theta, d_2 \sin \theta) = G_2 \left( \frac{\mathcal{M}_2}{\mathcal{M}_1} \cos \theta, \frac{\mathcal{M}_2}{\mathcal{M}_1} \sin \theta \right)$$

$$\mathbf{G}_3 \left( \frac{1 + d_2 \cos \theta}{2}, \frac{d_2 \sin \theta}{2} \right) = \mathbf{G}_3 \left( \frac{1 + \frac{\mathcal{M}_2}{\mathcal{M}_1} \cos \theta}{2}, \frac{\frac{\mathcal{M}_2}{\mathcal{M}_1} \sin \theta}{2} \right)$$

finally the distance  $d_3 = \sqrt{x^2 + y^2}$  can be computed:

$$d_3 = \sqrt{\frac{1}{4} + \frac{\mathcal{M}_2^2}{4\mathcal{M}_1^2} + \frac{\mathcal{M}_2}{2\mathcal{M}_1} \cos \theta} \quad (8)$$

### 6.3 Data taking from the position sensors

We collect the amplitude of the NCal support recoil motion when the NCal was rotating at 14 Hz. The counterweight should then give, depending on the mounting angle, a displacement greater or lower than the 13  $\mu\text{m}$  obtained with the rotor without counterweight.

The figure 10 shows this amplitude as a function of the mounting angle of the counterweight on the rotor. The black dotted points represent the data from the motion sensors, the red line is a fit on the data using the model from equation 8 and the blue line is the same model assuming the ratio between  $\mathcal{M}_2$  and  $\mathcal{M}_1$  is equal to 1 (i.e a counterweight with the correct moment but with different mounting angles).

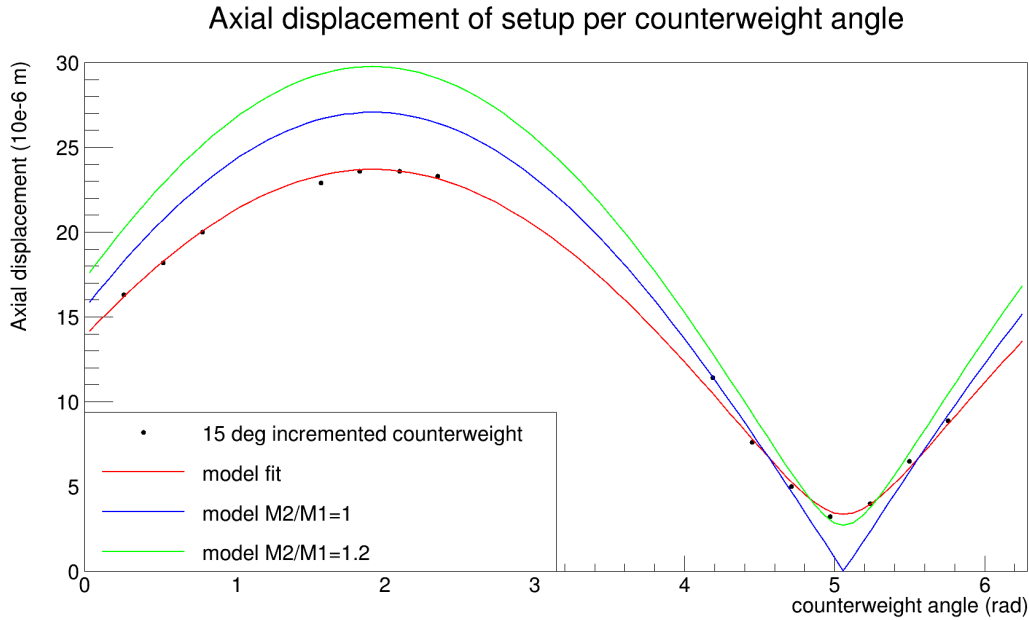


Figure 10: Amplitude of the axial displacement as a function of the angle of the counterweight. Data is shown as black dots, then fitted using the model in red, the blue line shows the model assuming the ratio between moments  $\mathcal{M}_1$  and  $\mathcal{M}_2$  is equal to 1, the green line shows the model assuming the moments ratio is 1.2.

The blue line gives the minimum displacement of 0  $\mu\text{m}$  for an angle of 5.06 rad or 289.9°. This angle is therefore where the counterweight should be placed to compensate the moment of the unbalanced rotor. The green line represents the moments ratio equal to 1.2, this shows that in our case the ratio is below 1.

We have to note that the number of screws used was not always the same and their position neither, meaning that the data taking is a bit less precise than if all four screws were used for every measure. This issue has to be taken into account as the correction gets more precise.

## 6.4 Counterweight tuning

In this section we will discuss about the making of a stainless steel counterweight using the results from last section.

### 6.4.1 Machined circular plate

The purpose of a stainless steel counterweight is that the higher density of the material makes the counterweight more massive for the same dimensions to limit the material to be removed from the counterweight and keep enough screw/holes. In a first place, a circular plate is machined as shown in figure 11.

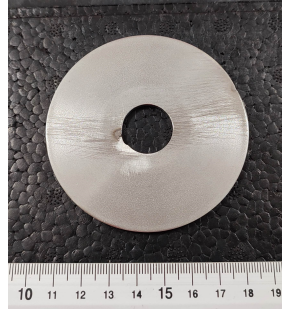


Figure 11: Machined circular stainless steel plate.

It is designed to be the same inner and outer radius as the aluminum plate (10 mm and 40 mm).

### 6.4.2 Determination of the geometry of the counterweight

From figure 10 the model fit gave  $\mathcal{M}_2/\mathcal{M}_1 = 0.75$  while the targetted result is  $\mathcal{M}_2/\mathcal{M}_1 = 1$  so we must have  $\mathcal{M}_1 = \mathcal{M}_2 = m d_1/0.75 = 3.63 \times 10^{-4}$  kg.m ( $m$  being the required mass for the counterweight and  $d_1$  its center of gravity). Assuming the center of gravity of the counterweight would be the following:

$$d = \frac{\rho}{m} \int_r^R \int_0^\theta \int_0^h r dV \quad (9)$$

with the parameters:

$$\rho = 7776 \text{ kg.m}^{-3}$$

$$r = 10.04 \times 10^{-3} \text{ m and } R = 39.95 \times 10^{-3} \text{ m}$$

$$h = 2.00 \times 10^{-3}$$

These are the mean values of each measured parameter, stainless steel is harder to machine than aluminum therefore the dimensions are less precise.

Now we have this equation for  $\mathcal{M}_1$ :

$$\mathcal{M}_1 = dm = \rho \iiint r dV = 3.63 \times 10^{-4} \text{ kg.m} \quad (10)$$

By computing eq. (10) we find  $\theta = 64.04^\circ$ , resulting in the geometry shown in figure 12.

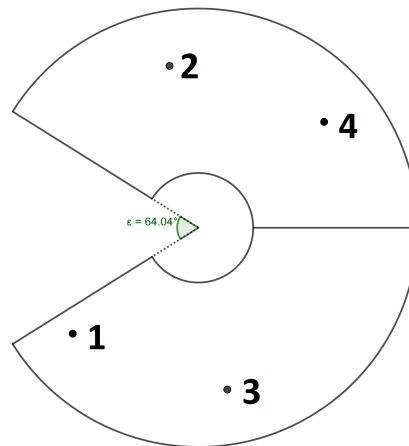


Figure 12: Geometry of the stainless steel counterweight to be machined. The computed opening angle has a value of  $64.04^\circ$ . Screw holes are labelled from 1 to 4.

### 6.4.3 Testing the theoretical geometry

Now that the theoretical geometry has been determined, we have to test the machined counterweight and check if any adjustment is necessary.

The tests shown that the geometry gave a lower axial displacement value than the minimum of the data from figure 10 with values between  $2.0 \mu\text{m}$  and  $2.9 \mu\text{m}$  depending on the location of the screws. The fact that the results did not give a value of displacement closer to zero can be explained by:

- The number and placement of the screws was not taken into account during the preliminary tests making the measures slightly uneven (a screw weighs below 1 g).
- The theoretical model does not include screw holes.
- The stainless steel plate was roughly machined, the thickness and diameter values were averaged to mean values.

A further correction is therefore needed to achieve a lower axial displacement.

### 6.4.4 Final corrections on the counterweight

During further tests we noticed that the residual recoil motion was less than  $0.4 \mu\text{m}$  with a configuration of one large screw and eight nuts on hole 4 and one medium screw and one nut on hole 3 (the screw holes are the ones labelled on figure 10). Weighing the screws and nuts revealed that we needed to remove material equal to 4.1 g of material on the opposite of hole 4 (hole 1) and 1.5 g of material on the opposite of hole 3 (hole 2).

Considering the actual geometry of the counterweight shown on figure 12 we reduced the material on the counterweight as shown on figure 13. Since the quantity of material needed to be removed is larger on hole 1 than hole 2, the shape of the cuts are very different (one section of disk is removed on hole 1 while only a small external layer is removed above hole 2 on figure 13).

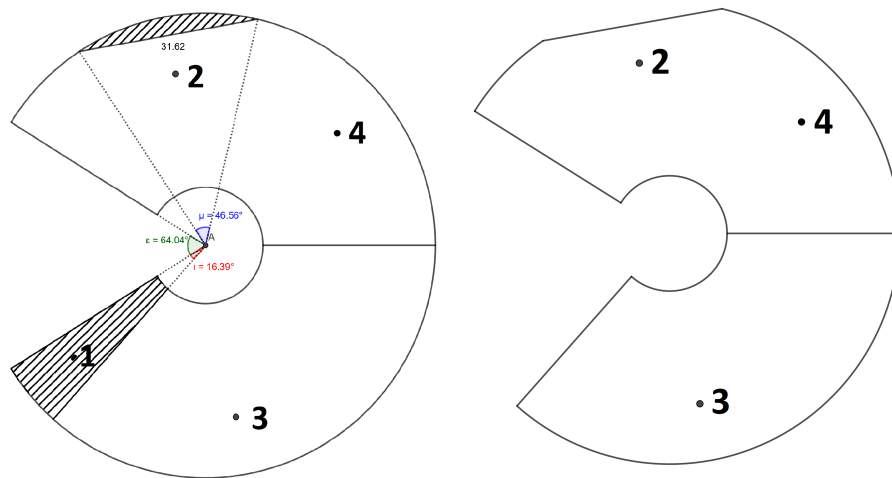


Figure 13: Final geometry of the counterweight with trimmed material located on screw hole 1 and next to hole 2. Left is the geometry of the counterweight with the cuts displayed as hatched areas, right is the remaining material on the counterweight after the cuts.

This last counterweight geometry was tested and resulted in recoil motion of just above  $1 \mu\text{m}$  using four small screws. We managed to reduce this value below  $0.4 \mu\text{m}$  while testing this geometry with a larger screw on hole 4 (and small screws on holes 1, 2 and 3). We consider this value to be acceptable for the balancing of the rotor.

## 7 Characterization of the rotor using an advanced model

### 7.1 Thickness

A more advanced model can be used considering the deformations on the surfaces of the sectors for better accuracy. Each measurement point of table 4 can be considered as a sub-sector with its own thickness.

The uncertainty on this value is more complex to evaluate. As a conservative approach we use the rms of the deviation to a plane ( $8.2 \mu\text{m}$  see section 4.1) to which we add linearly the uncertainty on the flatness of the measurement table ( $2.0 \mu\text{m}$ ) as well as the measurement tool ( $2.2 \mu\text{m}$ ). The total uncertainty on the thickness is  $13 \mu\text{m}$ .

### 7.2 Radius

On figure 3 we divided the external sectors in 4 sub-sectors for each sector (blue points). We convert the point of table 6 to the grid of figure 3 by averaging the two closest values and converting them to  $21.5^\circ\text{C}$ . The results are shown in table 8. We notice that the R sector is on average  $9 \mu\text{m}$  larger than the L sector.

Radius	L sector		R sector	
	Up	Down	Up	Down
1	104.024	104.024	104.036	104.037
2	104.039	104.037	104.044	104.044
3	104.039	104.037	104.044	104.044
4	104.024	104.024	104.036	104.037

Table 8: Radius measurements (in mm at 23°C) for the L and R sectors of R4-01.

The rms of the radii is  $7.5 \mu\text{m}$ . The tool uncertainty is  $2.4 \mu\text{m}$ . Like for the thickness we use a linear sum and find the uncertainty on both radii to be  $10 \mu\text{m}$ .

### 7.3 Chamfers on the rotor

The rotor has been machined with four chamfers on the inner radius as shown on figure 14 (see drawing at the end of the note). Adding the chamfers to the geometry is expected to lower the 2f signal. This effect will be studied using FROMAGE.

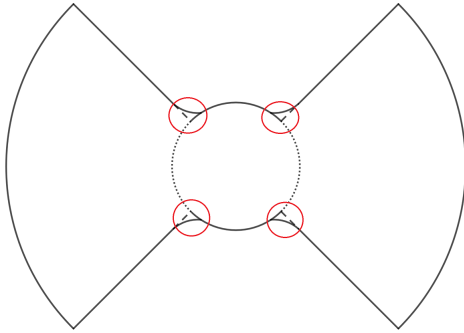


Figure 14: Outline of the rotor with the chamfers circled in red.

## 7.4 Expected NCal signals and uncertainties

### 7.4.1 Advanced model including chamfers and counterweight

The geometry used to describe the rotor as an advanced model is represented in figure 15. The external part of the sectors are divided in 2 sub-sectors each to correspond to the different radii determined. In addition we include the counterweight, the screws and screw holes.



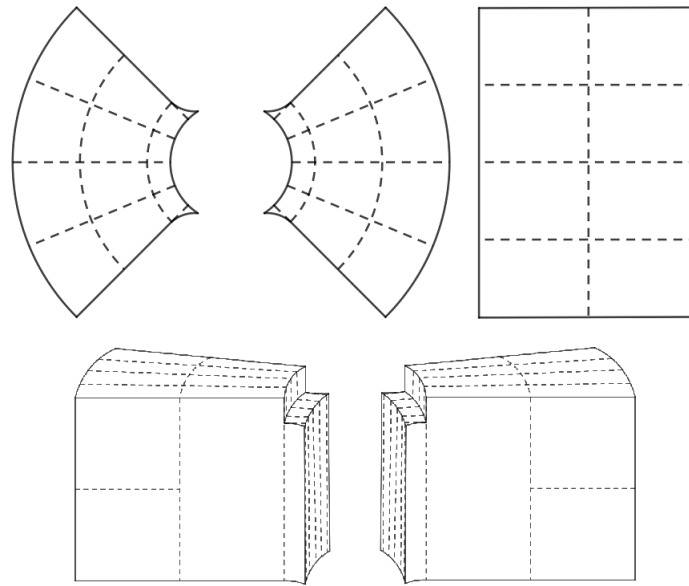


Figure 15: Advanced model geometry used to describe the rotor. Top left is a front view, top right is a side view (external sub-sectors) and bottom is a tilted view of the sectors. Only the 4 external part sectors are divided in 2 sub-sectors each. The chamfers are visible on the inner radius.

Using FROMAGE on this full geometry gives the following strains:

- $\text{strain}(1f) = \frac{8.0733 \times 10^{-20}}{(1f_{rot})^2}$
- $\text{strain}(2f) = \frac{2.1206 \times 10^{-18}}{(2f_{rot})^2}$
- $\text{strain}(3f) = \frac{2.4596 \times 10^{-23}}{(3f_{rot})^2}$

We can use FROMAGE to create files containing the position of each element to display them as shown on figure 16 (the grid used for the computation is the same as the one used for these images: 16x65x40 for the rotor and counterweight).

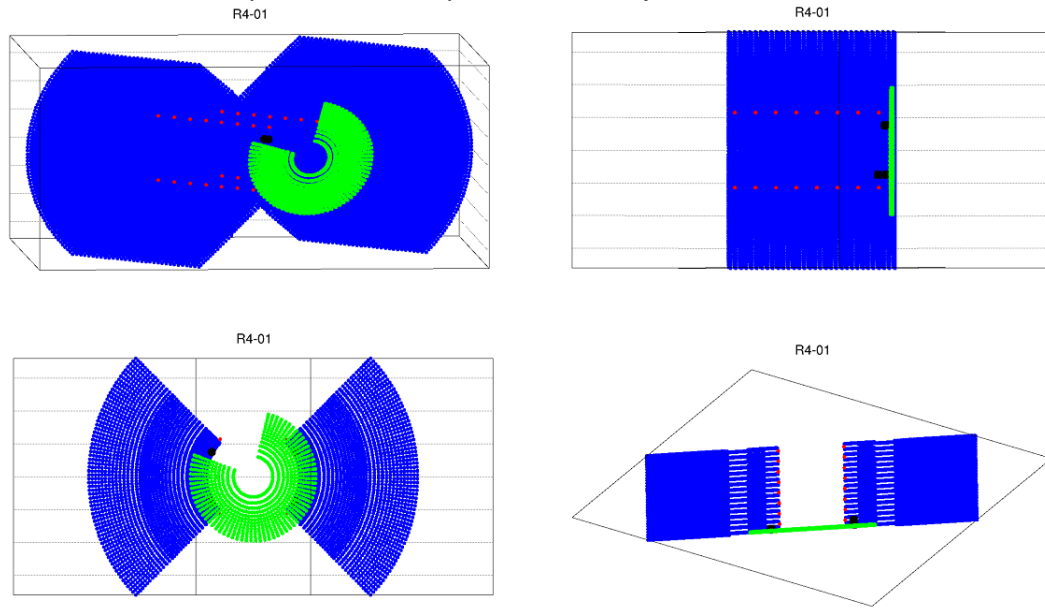


Figure 16: Cloud of points views of the position of each rotor and counterweight element from FROMAGE. Top left is a general view, top right is a side view, bottom left is a front view and bottom right is an upper view. The rotor sectors are shown in blue, the counterweight in green, the chamfers in red and the screws in black.

#### 7.4.2 Chamfers effect

Removing the chamfers from the advanced model we obtain the following strains:

- $\text{strain}(1f) = \frac{8.0738 \times 10^{-20}}{(1f_{rot})^2}$
- $\text{strain}(2f) = \frac{2.1208 \times 10^{-18}}{(2f_{rot})^2}$
- $\text{strain}(3f) = \frac{2.4596 \times 10^{-23}}{(3f_{rot})^2}$

The relative deviations from the advanced model are:

- (1f) : 0.006%
- (2f) : 0.009%
- (3f) : 0%

The chamfers have a small impact on the strain signals. The 2f and 1f signals decrease with the presence of chamfers. In the advanced model it is expected that the counterweight compensates some of the 1f signal from the chamfers so this geometry might not be complete.

#### 7.4.3 Counterweight effects using FROMAGE

Using FROMAGE we can compute the gravitationnal effect of the counterweight mounted on the rotor. We note that four screws were used to mount the counterweight on the rotor and have to be taken into account.

Table 9 shows the effects of each element considered on the advanced rotor model (without chamfers).

Geometry	strain/(1f) <sup>2</sup>	strain/(2f) <sup>2</sup>	strain/(3f) <sup>2</sup>
rotor	$5.0001 \times 10^{-21}$	$2.1202 \times 10^{-18}$	$2.2528 \times 10^{-23}$
rotor + screw holes	$5.0001 \times 10^{-21}$	$2.1201 \times 10^{-18}$	$2.2528 \times 10^{-23}$
rotor + counterweight (w. screws)	$8.0738 \times 10^{-20}$	$2.1209 \times 10^{-18}$	$2.4596 \times 10^{-23}$
rotor + counterweight (w.o screws)	$7.9462 \times 10^{-20}$	$2.1208 \times 10^{-18}$	$2.5050 \times 10^{-23}$

Table 9: Strain up to 3f for additional geometries of R4-01 including the counterweight.

The screw holes and screws have an effect below the grid uncertainty of FROMAGE (0.005% on 2f) and can be neglected in the 2f signal.

The presence of the counterweight (w. screws) induces the following relative deviations from the rotor without counterweight:

- $\sigma(1f) = 93.81\%$
- $\sigma(2f) = 0.033\%$
- $\sigma(3f) = 8.41\%$

The relative deviations on 1f and 3f are very large compared to the chamfers effect on the signal.

#### 7.4.4 Opening angles and sectors asymmetry

The counterweight is supposed to compensate the unbalance of the rotor at 1f. But that is not the case as it is shown in table 9. The likely explanation for that is an uncertainty on the opening angles and sector asymmetry that have not been accurately measured.

Since the thickness and radii of the sectors have been precisely measured we can check how the opening angle and the asymmetry of the center of mass between the sectors affects the 1f signal: Using FROMAGE we managed to reduce the "rotor + counterweight (w. screws)" 1f signal by one order of magnitude by playing on these parameters sector by sector. The sectors have been modified with the following parameters, assuming a fixed parameter (see figure fig. 17):

- The L sector has been rotated by 2.897 mrad clockwise and its opening angle increased by 1.377 mrad on the sandblasted side.
- The R sector opening angle has been decreased by 0.349 mrad on the sandblasted side.

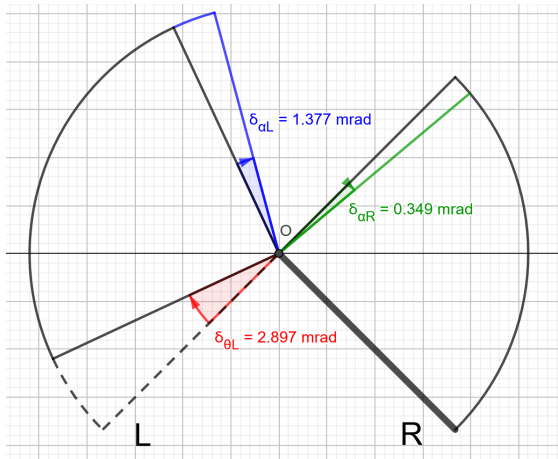


Figure 17: Modifications made in FROMAGE to compensate the 1f signal using the counterweight on the advanced rotor model. The L sector has been rotated clockwise by the angle  $\delta_{\theta L}$ . The opening angle of the L and R sectors have been respectively increase by  $\delta_{\alpha L}$  and decreased by  $\delta_{\alpha R}$ . The thick line represents the fixed radius on the R sector. The angle corrections have been magnified for visibility.

The geometry shown in fig. 17 including the counterweight (w. screws) and chamfers gives the following strains:

- $\text{strain}(1f) = \frac{7.3201 \times 10^{-21}}{(1f_{rot})^2}$
- $\text{strain}(2f) = \frac{2.1217 \times 10^{-18}}{(2f_{rot})^2}$
- $\text{strain}(3f) = \frac{2.5558 \times 10^{-22}}{(3f_{rot})^2}$

The relative deviation of this geometry from the section 7.4.1 is a 0.05% increase on the 2f signal. This deviation will be considered as the angle opening and asymmetry uncertainty.

The following formula represents how the opening angles  $\alpha_L$ ,  $\alpha_R$  and the angle between the center of mass of the sectors  $\Psi$  (see fig. 18) affects the 2f signal:

$$\begin{aligned} \text{strain}(2f) \propto & b_L \sin(\alpha_L) \cos(4\pi fT)(r_{max}^4 - r_{min}^4)_L \\ & + b_R \sin(\alpha_R) \cos(4\pi fT + 2\Psi)(r_{max}^4 - r_{min}^4)_R \end{aligned} \quad (11)$$

Using eq. (11) on a simple rotor model with identical sectors, all L/R indexed parameters are equal and  $\Psi = \pi$  giving  $\cos(\beta + 2\pi) = \cos(\beta)$  so both terms add each other for a maximum 2f signal (we find back the first order of eq. (6)).

In the case of  $\Psi = \frac{\pi}{2}$  we have  $\cos(\beta + \pi) = -\cos(\beta)$  so both terms cancel each other for a null 2f signal.

Our advanced model considers several sub-sectors of different thickness and radii, it is therefore possible to increase the 2f signal by playing with the opening angles  $\alpha_{L/R}$  and the angle  $\Psi$  in eq. (11). The maximum 2f signal can be obtained with  $\alpha_{L/R} \neq \pi/2$ .

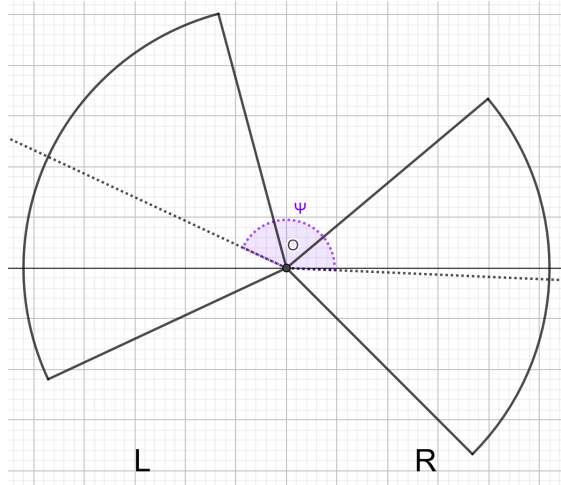


Figure 18: Angle  $\Psi$  between the center of mass of the sectors.

#### 7.4.5 Uncertainties

Comparing the advanced model of the rotor + chamfers ( $\text{strain}(2f) = 2.1202 \times 10^{-18}/(2f)^2$ ) to the simple model gives a relative deviation of 0.033%. This deviation will be considered as our modelling uncertainty.

The uncertainties considered for this full model are displayed in table 10.

R4-01 rotor parameter advanced model (23°C)			NCal 2f signal uncertainty	
name	mean value	uncertainty	formula	value (%)
Density $\rho$ (kg.m <sup>-3</sup> )	2808.0	0.2	$\delta\rho/\rho$	0.007
Thickness $b$ left sector (12 sub-sectors) (mm)	104.322	$1.26 \times 10^{-2}$	$\delta b/b$	0.012
Thickness $b$ right sector (12 sub-sectors) (mm)	104.307			
$r_{max}$ left sector (8 ext sub-sectors) (mm)	104.031	$9.9 \times 10^{-3}$	$4\delta r_{max}/r_{max}$	0.038
$r_{max}$ right sector (8 ext sub-sectors) (mm)	104.040			
$G$ (m <sup>3</sup> .kg <sup>-1</sup> .s <sup>-2</sup> )	$6.67430 \times 10^{-11}$	$1.5 \times 10^{-15}$	$\delta G/G$	0.002
Temperature $T$ (°C)	23	3	$\left  \frac{\partial h}{\partial T} \right  \frac{\Delta T}{h}$	0.014
Modelling Uncertainty				0.033
Angle opening and asymmetry uncertainty				0.050
Total uncertainty from the rotor (quadratic sum)				0.074

Table 10: Uncertainties on the amplitude of the calibration signal at 2f from the R4-01 rotor advanced model geometry at 23°C.

## A Appendix

```
### This is a cfg file for a more realistic geometry of the mirror and the Virgo O4 NCal (2022)
```

```
### ALL THE OBJECTS ARE DEFINED IN THE MIRROR'S FRAME (0,x,y,z),
### with 0 the center of the mirror, x axis along the ITF's beam toward the beam-splitter,
### y axis orthogonal to x in the plane of the ITF,
### z axis orthogonal to the plane of the ITF upward
```

```
### MIRROR DEFINITION
```

```
GRID_SIZE 12 30 8
```

```
CYLINDER 2202. 0 0.175 0.2 360 0 0 0
```

```
GRID_SIZE 1 1 1
```

```
# Defining the flats on the edge of the mirror
```

```
CUT_CYL 2202. 0.175 0.2 0.05 0 0
```

```
CUT_CYL 2202. 0.175 0.2 0.05 0 180
```

```
# Defining the ears and anchors of the mirror
```

```
CUBOID 2202. 0.090 0.010 0.015 0 0.1782 -0.0125
```

```
CUBOID 2202. 0.090 0.010 0.015 0 -0.1782 -0.0125
```

```
CUBOID 2202. 0.039 0.008 0.008 -0.02 -0.1772 -0.024
```

```
CUBOID 2202. 0.039 0.008 0.008 -0.02 0.1772 -0.024
```

```
CUBOID 2202. 0.039 0.008 0.008 0.02 -0.1772 -0.024
```

```
CUBOID 2202. 0.039 0.008 0.008 0.02 0.1772 -0.024
```

```
### ROTOR DEFINITION
```

```
# CYLINDER DENSITY INNER_RADIUS OUTER_RADIUS THICKNESS OPEN_ANGLE r z theta
```

```
ROTOR_CYLINDRICAL 1.7 34.7 0 0
```

```
## COUNTERWEIGHT 7776.
```

```
GRID_SIZE 16 65 40
```

```
CYLINDER 7776. 0.01004 0.03995 0.00200 279.57 0 0.049114 298.085
```

```
GRID_SIZE 1 1 1
```

```
CUT_CYL 7776. 0.03995 0.00200 0.03162 0 30
```

```
## SCREWS COUNTERWEIGHT
```

```
CYLINDER 7600. 0 0.0015 0.005 360 0.03 0.045614 150
```

```
CYLINDER -176. 0 0.0015 0.002 360 0.03 0.049114 30
```

```
CYLINDER 7600. 0 0.0015 0.003 360 0.03 0.046614 30
```

```
CYLINDER -176. 0 0.0015 0.002 360 0.03 0.049114 210
```

```
CYLINDER 7600. 0 0.0015 0.003 360 0.03 0.046614 210
```

```
CYLINDER -176. 0 0.0015 0.002 360 0.03 0.049114 330
```

```
CYLINDER 7600. 0 0.0015 0.010 360 0.03 0.043114 330
```

```
## SCREW HOLES
```

```
CYLINDER -2808.0 0 0.0015 0.012 360 0.03 0.046092 150
```

```
CYLINDER -2808.0 0 0.0015 0.012 360 0.03 0.0460875 30
```

```
CYLINDER -2808.0 0 0.0015 0.012 360 0.03 0.0460835 210
```

---

CYLINDER -2808.0 0 0.0015 0.012 360 0.03 0.0460665 330

# VERY FAST  
#GRID\_SIZE 4 4 4  
# FAST  
#GRID\_SIZE 8 17 14  
# SLOW  
#GRID\_SIZE 8 65 40  
# VERY SLOW  
GRID\_SIZE 16 65 40

## L sector  
## Inner part  
OUTER\_FILLET 2808.0 0.02893 0.101272 -0.003044 0.01 -11.125 146.25  
CYLINDER 2808.0 0.02893 0.03999 0.101276 22.5 0 -0.003044 146.25  
CYLINDER 2808.0 0.02893 0.03999 0.101269 22.5 0 -0.003051 168.75  
CYLINDER 2808.0 0.02893 0.03999 0.101264 22.5 0 -0.003044 191.25  
CYLINDER 2808.0 0.02893 0.03999 0.101259 22.5 0 -0.003044 213.75  
OUTER\_FILLET 2808.0 0.02893 0.101255 -0.003044 0.01 11.125 213.75

## Middle part  
CYLINDER 2808.0 0.03999 0.071989 0.104332 22.5 0 0 146.25  
CYLINDER 2808.0 0.03999 0.071989 0.104321 22.5 0 0 168.75  
CYLINDER 2808.0 0.03999 0.071989 0.104315 22.5 0 0 191.25  
CYLINDER 2808.0 0.03999 0.071989 0.104311 22.5 0 0 213.75

## Outer part  
CYLINDER 2808.0 0.071989 0.104024 0.05217308854 22.5 0 0.02608654427 146.25  
CYLINDER 2808.0 0.071989 0.104024 0.05217308854 22.5 0 -0.02608654427 146.25

CYLINDER 2808.0 0.071989 0.104039 0.05216859389 22.5 0 0.02608429694 168.75  
CYLINDER 2808.0 0.071989 0.104037 0.05216859389 22.5 0 -0.02608429694 168.75

CYLINDER 2808.0 0.071989 0.104039 0.05215866227 22.5 0 0.02607933114 191.25  
CYLINDER 2808.0 0.071989 0.104037 0.05215866227 22.5 0 -0.02607933114 191.25

CYLINDER 2808.0 0.071989 0.104024 0.05214823311 22.5 0 0.02607411656 213.75  
CYLINDER 2808.0 0.071989 0.104024 0.05214823311 22.5 0 -0.02607411656 213.75

## R sector  
## Inner part  
OUTER\_FILLET 2808.0 0.02893 0.101269 -0.003039 0.01 11.125 33.75  
CYLINDER 2808.0 0.02893 0.03999 0.101269 22.5 0 -0.003039 33.75  
CYLINDER 2808.0 0.02893 0.03999 0.101263 22.5 0 -0.003045 11.25  
CYLINDER 2808.0 0.02893 0.03999 0.101258 22.5 0 -0.003050 348.75  
CYLINDER 2808.0 0.02893 0.03999 0.101255 22.5 0 -0.003053 326.25  
OUTER\_FILLET 2808.0 0.02893 0.101255 -0.003053 0.01 -11.125 326.25

## Middle part  
CYLINDER 2808.0 0.03999 0.071989 0.104321 22.5 0 0 33.75  
CYLINDER 2808.0 0.03999 0.071989 0.104315 22.5 0 0 11.25  
CYLINDER 2808.0 0.03999 0.071989 0.104303 22.5 0 0 348.75  
CYLINDER 2808.0 0.03999 0.071989 0.104295 22.5 0 0 326.25

## Outer part  
CYLINDER 2808.0 0.071989 0.104036 0.05216653198 22.5 0 0.02608326599 33.75

---

CYLINDER 2808.0 0.071989 0.104037 0.05216653198 22.5 0 -0.02608326599 33.75

CYLINDER 2808.0 0.071989 0.104044 0.05215610282 22.5 0 0.02607805141 11.25  
CYLINDER 2808.0 0.071989 0.104044 0.05215610282 22.5 0 -0.02607805141 11.25

CYLINDER 2808.0 0.071989 0.104044 0.05214717127 22.5 0 0.02607358564 348.75  
CYLINDER 2808.0 0.071989 0.104044 0.05214717127 22.5 0 -0.02607358564 348.75

CYLINDER 2808.0 0.071989 0.104036 0.05214067648 22.5 0 0.02607033824 326.25  
CYLINDER 2808.0 0.071989 0.104037 0.05214067648 22.5 0 -0.02607033824 326.25

## GENERAL PARAMETERS

STEP 22.5 16

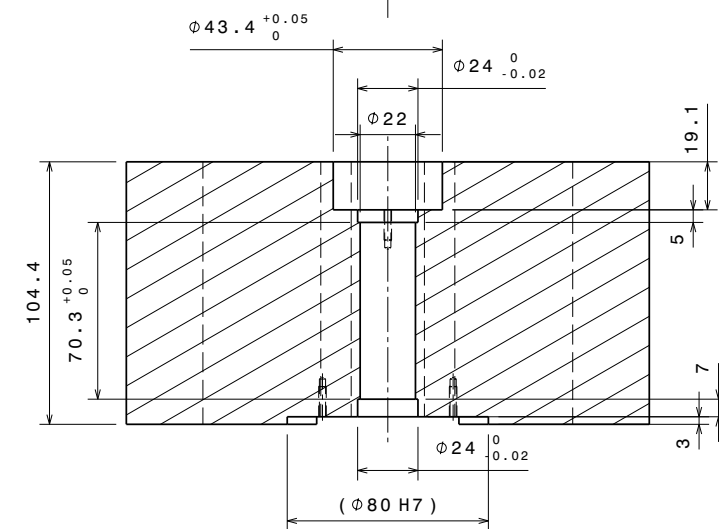
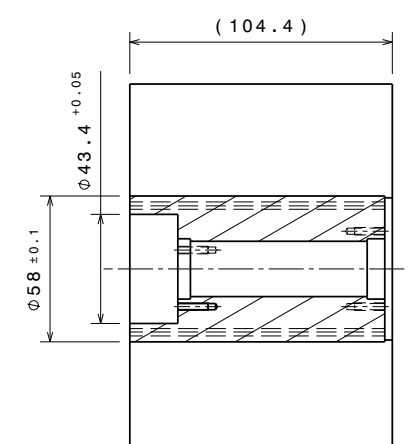
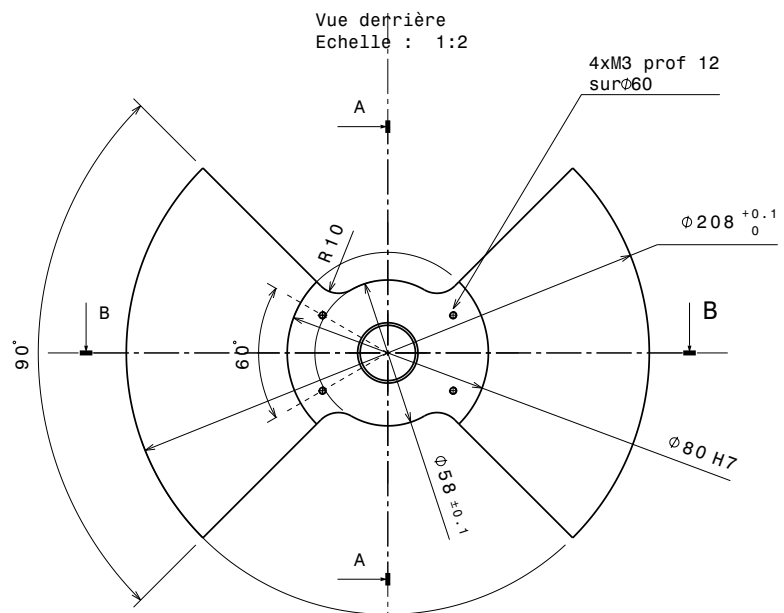
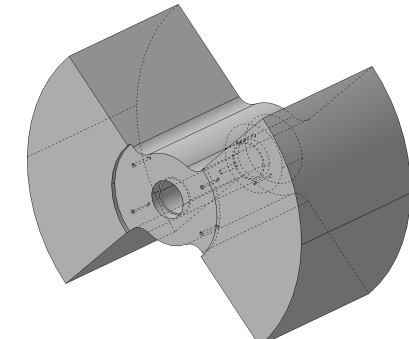
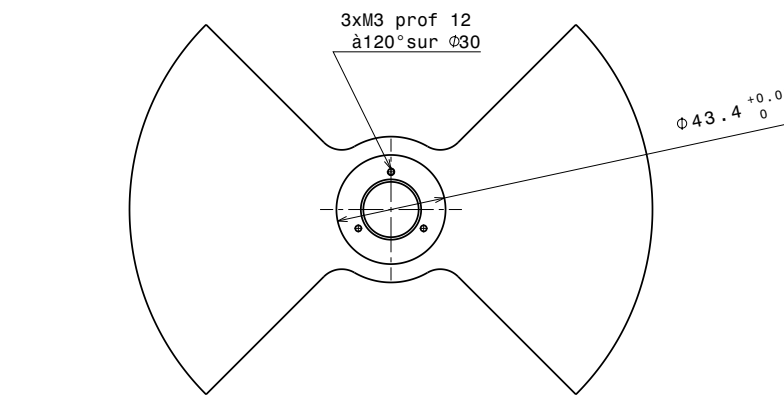
ARM\_LENGTH 3000


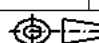
SIGNAL 3

## SAVE FILES

SAVE\_ROTOR R4-01\_rotor





1		AW-7075	5		
N°	Qté	Matière	Traitement de surface	Masse Kg	Dessin d'ensemble
Rug. gén. : Ra = 1,6		Tol. gén. : ISO 2768 mK	Chanfreins: 0,2 à 45°	Projet :	VIRGO Ncal
CNRS - IN2P3		ROTOR_S			
		Dessiné par :	Vérifié par :	A3	Numéro
		V. Zeter			Echelle 1:2
23, rue du Loess - BP 28 67037 Strasbourg Cedex 02		19/11/2021			

Copyright IN2P3 TIRoS